# Pre-TCR ligand binding impacts thymocyte development before αβTCR expression

Robert J. Mallis[a,1], Ke Bai[b,1], Haribabu Arthanari[a], Rebecca E. Hussey[c], Maris Handley[c], Zhenhai Li[b], Loice Chingozha[d], Jonathan S. Duke-Cohan[c,e], Hang Lu[d], Jia-Huai Wang[a,c,f], Cheng Zhu[b], Gerhard Wagner[a], and Ellis L. Reinherz[c,e,2]

[a]Department of Biological Chemistry and Molecular Pharmacology, Harvard Medical School, Boston, MA 02115; [b]Coulter Department of Biomedical Engineering, Georgia Institute of Technology, Atlanta, GA 30332; [c]Department of Medical Oncology, Laboratory of Immunobiology, Dana-Farber Cancer Institute, Boston, MA 02115; [d]School of Chemical and Biomolecular Engineering, Georgia Institute of Technology, Atlanta, GA 30332; [e]Department of Medicine, Harvard Medical School, Boston, MA 02115; and [f]Department of Pediatrics, Harvard Medical School, Boston, MA 02115

Edited by Kenan Garcia, Stanford University, Stanford, CA, and approved May 14, 2015 (received for review March 11, 2015)

**Adaptive cellular immunity requires accurate self- vs. nonself-discrimination to protect against infections and tumorous transformations while at the same time excluding autoimmunity. This vital capability is programmed in the thymus through selection of αβT-cell receptors (αβTCRs) recognizing peptides bound to MHC molecules (pMHC). Here, we show that the pre-TCR (preTCR), a pTα-β heterodimer appearing before αβTCR expression, directs a previously unappreciated initial phase of repertoire selection. Contrasting with the ligand-independent model of preTCR function, we reveal through NMR and bioforce-probe analyses that the β-subunit binds pMHC using Vβ complementarity-determining regions as well as an exposed hydrophobic Vβ patch characteristic of the preTCR. Force-regulated single bonds akin to those of αβTCRs but with more promiscuous ligand specificity trigger calcium flux. Thus, thymic development involves sequential β- and then, αβ-repertoire tuning, whereby preTCR interactions with self pMHC modulate early thymocyte expansion, with implications for β-selection, immunodominant peptide recognition, and germ line-encoded MHC interaction.**

pre–T-cell receptor | NMR spectroscopy | biomembrane force probe | thymic development | repertoire selection

The thymus provides discrete microenvironments for both commitment and stepwise maturation of multipotent hematopoietic progenitors to the T lineage. The earliest progenitors enter at the corticomedullary junction as CD4−CD8− [double-negative (DN)] CD44+CD25− (DN1) cells, extensively proliferate, and consecutively progress through DN2 (CD4−CD8−CD44+CD25+), DN3 (CD4−CD8−CD44−CD25+), and DN4 (CD4−CD8−CD44−CD25−) stages in the outer cortex before becoming CD4+CD8+ double-positive (DP) cortical thymocytes, where proliferation is largely curtailed (1, 2). T-cell receptor-β (TCRβ) gene locus rearrangement and expression first occur at the DN3 stage, whereas those of the TCRα locus follow at the DP stage. At the DN stages, Notch without and then with pre-TCR (preTCR) signaling facilitates proliferation and differentiation, whereas at the DP stage, αβTCR signaling is key for developmental progression (reviewed in ref. 3). Repertoire selection eliminates useless (nonselectable) or potentially dangerous (strongly self-reactive) TCR specificities and is initiated at the DP stage, processes referred to as death by neglect and negative selection, respectively. Contemporaneously or temporally bracketing those processes, positive selection gives rise to CD4+CD8− and CD4−CD8+ single-positive thymocytes. Positively selected cells migrate to the thymic medulla to complete selection and functional maturation before peripheral egress as T lymphocytes. Within the medulla, CD4+ single-positive thymocytes undergo transcriptional regulator autoimmune regulator (AIRE)-dependent negative selection (4).

Running the thymic selection gauntlet is an arduous process, with only 1% or less of the preselection TCR repertoire observed in the postselection compartment (5). Furthermore, subpopulation kinetic analysis reveals that, although early progenitors give rise to 50 million thymocytes per day in the mouse, only 1 million thymocytes exit to the peripheral lymphoid compartment (6). Chemokines as well as plexin–semaphorin interactions orchestrate movement of thymocytes along the various developmental niches (7–9).

The first major checkpoint in early thymic development is referred to as β-selection, where signaling through the preTCR terminates β-locus rearrangements, rescues cells from apoptosis, and induces significant additional expansion of progenitors (10). Through this process, DN thymocytes are enabled to differentiate to DP thymocytes, facilitating TCRα gene rearrangementsand the generation of millions of αβTCRs encoding distinct specificities for peptides bound to MHC molecules (pMHC) through paired Vα and Vβ domains of the TCR V module (ref. 11 and references therein). Earlier work in vitro and in vivo (12) has suggested that preTCR signaling function is autonomous. Based on lattice packing in an X-ray crystallographic study, it was further speculated that the activated preTCR might form a superdomain of two preTCRs sitting close to the membrane in an antiparallel fashion with ligand binding precluded (13). However, the murine preTCR possesses an additional glycan at pTα N101, which would prevent formation of such a superdomain. In addition, recent β-chain X-ray structures (14) suggest a preTCR model where the receptor, with a Vβ domain that is not paired with Vα, can, nevertheless, extend from the thymocyte membrane in an upright orientation as a monomer or dimer, providing an alternative model of preTCR function.

Given that camelids possess a functional class of antibodies devoid of light chain (15) (unlike typical antibodies with paired

## Significance

**The thymus generates the repertoire of disease-fighting T lymphocytes, affording lifelong host protection against infectious organisms and other pathogens. To achieve this goal, a microinductive environment converts precursors into millions of distinct functional T cells. Because each T lineage cell displays a clone-specific T-cell receptor (TCR) that is generated through stochastic (i.e., haphazard) recombination events, the specificities of thymocytes must be interrogated, and those expressing useless or harmful TCRs are removed before their exit from the thymus. Here, we show that repertoire selection begins at a stage preceding the one currently identified. The pre–T-cell receptor, previously thought to operate autonomously, has robust ligand binding behavior to initiate the first stage of this process.**

Author contributions: R.J.M., H.A., C.Z., G.W., and E.L.R. designed research; R.J.M., K.B., H.A., R.E.H., M.H., Z.L., and L.C. performed research; R.J.M., K.B., H.A., M.H., Z.L., L.C., J.S.D.-C., H.L., J.-H.W., C.Z., G.W., and E.L.R. analyzed data; and R.J.M., K.B., J.S.D.-C., C.Z., G.W., and E.L.R. wrote the paper.

The authors declare no conflict of interest.

This article is a PNAS Direct Submission.

See Commentary on page 8166.

[1]R.J.M. and K.B. contributed equally to this work.

[2]To whom correspondence should be addressed. Email: ellis_reinherz@dfci.harvard.edu.

This article contains supporting information online at www.pnas.org/lookup/suppl/doi:10.1073/pnas.1504971112/-/DCSupplemental.

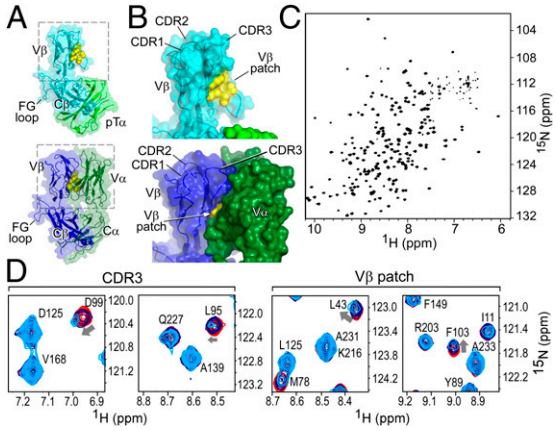


**Fig. 1.** The structure of the β-subunit when incorporated into pTαβ or TCRαβ heterodimers suggests that the preTCR has ligand binding properties. (*A* and *B*) Structures of the (*Upper*) pTα/LC13β preTCR [Protein Data Bank (PDB) ID code 3OF6] and (*Lower*) N15αβTCR (PDB ID code 1NFD) heterodimers. (*A*) The overall fold of β remains consistent within pTαβ compared with within TCRαβ. (*B*) Highlight of Vβ domain and CDR loops within pTαβ and αβTCR. The hydrophobic Vβ patch, which is exposed in pTαβ but not in TCRαβ, is shown in yellow. (*C*) TROSY-HSQC spectrum of N15β (with backbone residue assignments overlaid in Fig. S1*B*) showing spectral dispersion consistent with the β sheet-rich fold of the β-subunit. (*D*) Select regions of overlaid TROSY-HSQC spectra of 200 μM $^{1}$H-$^{15}$N N15β alone (red) and with the addition of 200 (blue) or 500 μM (cyan) unlabeled VSV8/K$^{b}$. Chemical shift changes are highlighted for residues D99 and L95 of CDR3 and L43 and F103 of the Vβ patch. Note the lack of changes in C-domain residues, for example, D125, A139, V168 or A233.

heavy and light chains) and that antibody $V_H$ domains in mammals are often major determinants of antigen affinity and specificity (16), we reasoned that the Vβ could be capable of interacting with pMHC ligands. It has already been observed that endogenous retroviruses and bacterial superantigens interact independently with mature αβTCR Vβ domains (17). We, thus, hypothesized that ligand binding could have an effect on pTα-β–mediated early thymic development, with the potential for β to bind ligand, using the canonical complementarity determining region (CDR) loops as well as the exposed Vβ patch region. In this study, we report that the preTCR shows all of the hallmarks of a functional receptor, with ligand binding, specificity tied to CDR loops, and functional effects linked to ligand binding regions. Furthermore, we are able to measure single-bond properties of preTCR–pMHC interactions to show that the preTCR maintains mechanical characteristics now known to be important for mature αβTCR function (18, 19).

## Results

**PreTCRβ Subunit Displays Structural Elements with Potential for Antigen Recognition.** The structures of TCRβ subunits (i.e., chains) are quite similar in conformation of CDR loops and the Cβ FG loop, whether they are part of pTα-β (13) or TCRαβ heterodimer (20) (Fig. 1*A*) or alone (14, 21). Additionally, the preTCR unmasks a hydrophobic patch (13, 14) of Vβ that is not surface-exposed on the mature TCRαβ molecule (Fig. 1*B*). Using NMR methods to examine N15β (22) in isolation, we found it to be folded (Fig. 1*C*) with a well-dispersed $^{1}$H-$^{15}$N transverse relaxation optimized spectroscopy (TROSY)-heteronuclear single quantum coherence (HSQC) spectrum. Three point mutations (Table S1) within the Cβ domain were made to ensure that nonspecific binding did not occur at the hydrophobic pTα– or Cα–Cβ interface site (20) (Fig. 1*A*) that is inaccessible in all surface-expressed preTCR or TCR molecules. NMR backbone assignment coverage (Fig. S1 *A*–*C*) was sufficient to allow us to test binding of this and N30β, which uses an entirely different Vβ germline segment (Vβ13 vs. Vβ5.2 for N15β), for recognition of the cognate ligand of their respective TCRαβ receptors: the vesicular stomatitis octapeptide (VSV8) bound to K$^{b}$ (VSV8/K$^{b}$) (22).

**β-Chain Interaction with pMHC Revealed by NMR Chemical Shift Titration Analysis.** In NMR-based titration experiments, where unlabeled VSV8/K$^{b}$ was added to $^{15}$N-labeled N15β, there were significant chemical shift changes within only the Vβ domain, indicating an interaction in solution (Figs. 1*D* and 2 *A* and *B* and Fig. S2*A*) (23). Additionally, there was a loss of intensity for those residues at the binding interface (Figs. 1*D* and 2*A* and Fig. S2*A*), suggesting an interaction in the intermediate exchange regime for NMR measurements, with exchange rates on the order of 1–100 s$^{-1}$ (23). The region affected by the binding event seems to include the assigned CDR1, CDR3, and the Vβ patch (14, 20) (Fig. 1 *A* and *B* and Fig. S2*A*). The Vβ patch is notably

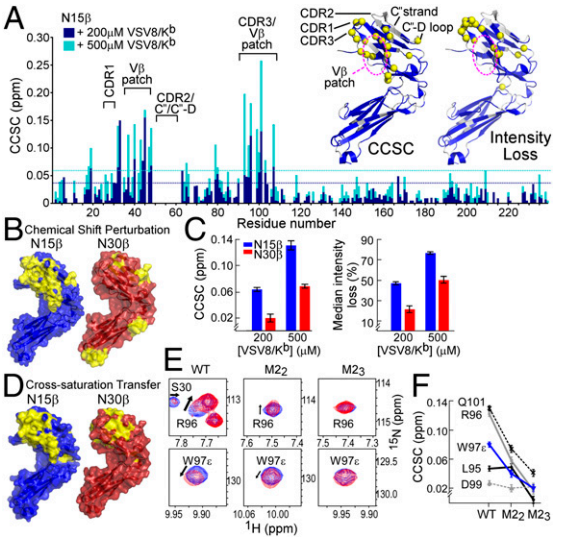


**Fig. 2.** β-Interaction with pMHC in solution as characterized by NMR. (*A*) The 2D $^{1}$H-$^{15}$N HSQC spectra of $^{15}$N-N15β were acquired alone or with 200 (dark blue bars) or 500 μM (light blue bars) VSV8/K$^{b}$. Combined $^{1}$H and $^{15}$N chemical shift change (CCSC) was calculated for each residue. Dotted lines, which are color-coded like bars, indicate 1 SD above median CCSC. *Inset* is the ribbon representation [Protein Data Bank (PDB) ID code 3Q5Y] of (*Left*) CCSC analysis or (*Right*) intensity loss (detailed in Fig. S2*A*) of VSV8/K$^{b}$ interaction with N15β. Amide protons exhibiting (*Left*) significant CCSCs or (*Right*) intensity losses are shown in yellow spheres in *Inset*. Regions corresponding to unassigned residues are white. (*B*) Solvent accessible surface representations of (*Left*) N15β (PDB ID code 3Q5Y) and (*Right*) N30β (PDB ID code 3Q5T) ectodomains with significant CCSCs colored yellow on surfaces within 6 Å of measured HN; β- and VSV8/K$^{b}$ concentrations were 200 μM. Similar results were obtained at 500 μM ligand (Fig. S2). β Is shown rotated ~120° about the *y* axis relative to Fig. 1 *A* and *B*. (*C*) Comparison of N15β and N30β interaction with VSV8/K$^{b}$. (*Left*) The 95th percentile of CCSC on mixing 200 or 500 μM VSV8/K$^{b}$ with 200 μM N15β or N30β. Error bars indicate SD of CCSC for peaks not affected by ligand addition. (*Right*) Median peak intensity losses of spectral peaks on addition of 200 or 500 μM VSV8/K$^{b}$ to 200 μM N15β or N30β. Error bars indicate propagated error using noise levels within NMR spectra. (*D*) Cross-saturation analysis. Surface representations of (*Left*) N15β and (*Right*) N30β ectodomains, with surfaces within 6 Å of HN exhibiting significant cross-saturation losses (detailed in *SI Materials and Methods*) shown in yellow. Representative spectral data and details of interacting surfaces are in Fig. S3 *C*–*E*. (*E* and *F*) Chemical shift perturbation of βCDR3 residues among N15β and CDR2 mutants. (*E*) Spectral regions of $^{1}$H-$^{15}$N TROSY-HSQC showing R96 or W97ε within CDR3 in the presence (red) or absence (blue) of VSV8/K$^{b}$ for N15β, M2$_2$, or M2$_3$. Arrows show directions of change in chemical shift; smaller changes are seen for the CDR2 mutants than for the WT. (*F*) CCSC of indicated CDR3 residues is less with VSV8/K$^{b}$ addition for M2$_2$ or M2$_3$ CDR2 variants vs. the WT N15β. Near-complete backbone assignments for M2$_2$ and M2$_3$ are shown in Fig. S1 *D*–*F*.

hydrophobic and contains conserved residues uniquely exposed in the preTCR (Fig. S3*A*) (13, 14). For N30β, the largest chemical shift changes on interaction in solution are not localized to a particular region but rather, distributed throughout the molecule (Fig. 2*B* and Fig. S2*B*) as are resonance peak intensity losses (Fig. S2*B*). With the exception of the N30β C″D loop, the magnitude of the largest chemical shift changes (Fig. 2*C* and Fig. S2) is lower for N30β than for N15β along with the median losses of peak intensity (Fig. 2*B* and Fig. S2) as the β-subunit forms a complex with pMHC and increases in size from 27 to 71 kDa (23). Taken together, these data lead us to conclude that pMHC binding to Vβ CDRs or patch is weaker for N30β than for N15β, because interactions with these elements are not specifically detected using chemical shift change or intensity measurements. Median intensity losses (Fig. 2*C*) similarly argue that the affinity is lower for N30β than for N15β. NMR-based titration of N15β with VSV8/K$^b$ yielded a $K_d = 390 \pm 50$ μM (Fig. S3*B*), a 3D (i.e., solution) affinity well within the range known to have a physiologic influence on T-cell signaling (24).

**Identification of the pMHC Binding Surface on the β-Chain Through Cross-Saturation Analysis.** To confirm the identity of the interaction contact surface, we used cross-saturation NMR, a technique that highlights areas of direct contact between molecules, unlike chemical shift analysis, which will also reflect allosteric- or self-association–induced changes in residue position (25). Cross-saturation NMR reveals that the binding of N15β with VSV8/K$^b$ (Fig. 2*D* and Fig. S3 *C* and *D*) occurs directly through the same Vβ residues highlighted in the chemical shift change experiment (Fig. 2 *A* and *B*). Surprisingly, a direct interaction of N30β with VSV8/K$^b$ (Fig. 2*D* and Fig. S3*E*) was detected in an area of the Vβ limited to CDR1 and -2 residues as well as a part of the Vβ patch. These binding surfaces in N15β and N30β are not compatible with a Vβ-mediated dimerization model (13, 14) in ligand recognition. Although the data show that chemical shift changes are more broadly dispersed throughout N30β (Fig. 2 *A* and *B*), these events are consequent to secondary or nonspecific interactions rather than highlight a direct contact site with VSV8/K$^b$. Most importantly, the results suggest that, between these two β-subunits, a common interaction motif exists that supports a weaker interaction with VSV8/K$^b$ in N30β than in N15β.

**CDR Residues Are Involved in β-Chain Binding to pMHC.** Mutational analysis of the direct interaction between N15β and VSV8/K$^b$ supports an important role for CDR residues in mediating a specific interaction. For example, N15β CDR2 mutants $M2_2$ (Y50A/E51A) and $M2_3$ (Q48A/Y50A/E51A) (NMR backbone assignments in Fig. S1 *D*–*F*) show decreased binding to VSV8/K$^b$ as evidenced by reduced chemical shift perturbations of CDR3 residues (Fig. 2 *E* and *F*). Similarly, N15β CDR3 mutant W97A showed decreased binding relative to N15β WT when median intensity losses are compared (Fig. S4*A*). Confirming the specificity, no significant interaction was observed when N15β WT was mixed with Ig fold-containing protein CD3γε (Fig. S4*A*). Although backbone assignments could not be obtained for the full-length VSV8/K$^b$ (26), using $^{15}$N-labeled H-2K$^b$ heavy chain bound to unlabeled VSV8 and β2m, we were able to observe chemical shift changes and line broadening when N15β was added in increasing concentrations, analogous to that seen with labeled N15β (Fig. S4 *B*–*D*). Overall, the interaction between N15β or N30β and VSV8/K$^b$ suggests contributions of conserved, germ line-encoded β-MHC binding events, consistent with prior reports (27, 28) but extending to the preTCR. This interaction may be further modulated by variable CDR3 residues as well as Vβ patch residues within N15β and N30β.

**Single-Bond Lifetime Analysis of Complete preTCRs with pMHC Ligands Uncovers Broadened Specificities.** Micropipette and biomembrane force-probe (BFP) analyses can be implemented to measure in situ binding affinity, kinetic rates, and force-dependent single-bond lifetimes between cell surface receptors and their ligands using an approach entirely orthogonal to solution methods (18). We used various pMHC ligands to ascertain if any interaction is observed with preTCR on retrovirally transduced SCID.adh immature (CD4$^-$/CD8$^+$) thymocytes, which lack TCRα and -β chains but express all CD3 subunits and pTα. Biotinylated VSV8/K$^b$ was bound to the surface of a micropipette-aspirated RBC or a glass bead attached to the RBC apex and used to analyze binding with SCID.adh cells expressing N15αβTCR, pTα/N15β WT, pTα/N30β WT, or indicated preTCR variants on the surface (Fig. 3*A* and Fig. S5 *A*–*D*). To exclude coreceptor influences, a K$^b$ variant lacking CD8 binding was used throughout (18). Binding events were observed for N15αβTCR, N15β WT, mutants, and N30β WT (Fig. 3*A*), with N15β WT possessing the highest 2D affinity of the tested preTCRs. No binding occurred in control cells lacking TCRα and -β (Fig. S5*E*). The specificity of the N15αβTCR is considerably more precise than that of WT or mutant N15β-containing preTCRs, where interactions with cognate VSV8/K$^b$ and OVA/K$^b$, gp66/I-A$^b$, or Hb/I-E$^k$ are more similar (Fig. 3*A*). Intriguingly, N15β $M2_3$ seems to possess increased cross-reactivity compared with WT or $M2_2$ (Fig. 3*A*), suggesting that the mutation of residue Q48 relieves some constraints on specificity. Mutagenesis of the β-patch region (N15β patch triple mutant $MP_3$)

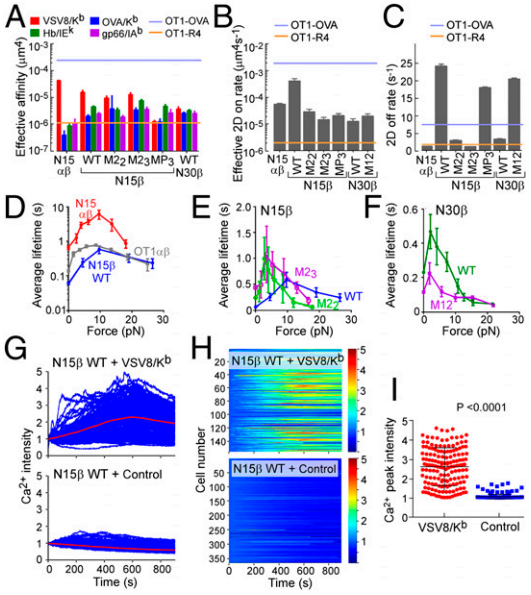


**Fig. 3.** Biophysical characterization of pMHC binding to and signaling by cell surface preTCR. (*A*) Effective 2D affinity was calculated from adhesion frequencies of each of the indicated receptors with the cognate ligand VSV8/K$^b$, an unrelated peptide bound to the same allele of MHCI (OVA/K$^b$), or unrelated peptides bound to two MHCII alleles (gp66/I-A$^b$ and Hb/I-E$^k$). Shown for reference are the 2D affinities for the OT1 αβTCR interaction with its cognate peptide ligand OVA/K$^b$ or the weak Arg-substituted altered peptide ligand R4/K$^b$. (*B* and *C*) Effective (*B*) 2D on rates and (*C*) 2D off rates for preTCRs compared with N15αβ. Shown for reference are the 2D rates for the OT1 αβTCR interaction with OVA/K$^b$ or the altered peptide ligand R4/K$^b$. (*D*–*F*) Average bond lifetime measures of cell surface N15β WT, N30β WT, N15β variant preTCRs, or N15αβTCR binding to VSV8/K$^b$ as a function of force. (*D*) N15αβ vs. N15β WT. The lifetimes of OT1 αβTCR-OVA/K$^b$ interaction are shown for comparison. (*E*) N15β WT vs. $M2_2$ and $M2_3$. (*F*) N30β WT vs. N30β M12. (*G*–*I*) $Ca^{2+}$ triggering of preTCR-expressing cells by VSV8/K$^b$ in a microfluidic cell trap chip. (*G*) Superposition of individual $Ca^{2+}$ response traces for N15β WT on exposure to (*Upper*) VSV8/K$^b$ or (*Lower*) BSA control-treated surfaces. (*H*) Heat map showing individual $Ca^{2+}$ responses, which are indicated by the colorimetric scaling of relative fluorescence signal in arbitrary units for data shown in *G*. (*I*) Maximal $Ca^{2+}$ intensities for individual cells from *G* and *H*. *P* value was determined using Student's *t* test.

strongly affects binding to $K^b$ ligands VSV and OVA while not adversely affecting interaction with either pMHCII ligand. Each preTCR tested exhibits unique kinetic properties, with the N15β WT possessing the highest on rate, although this on rate is tempered by a concomitant faster off rate (Fig. 3 *B* and *C*). Notwithstanding, the 2D affinity of the preTCR for its ligands is comparable with the weak OT1 TCR-R4/$K^b$ altered peptide ligand interaction that mediates positive selection of OT1 αβTCR transgenic thymocytes (29), implying that such measured preTCR–ligand interactions might be important in thymocyte fate involving preTCR-expressing DN thymocytes (vide infra). This R4 peptide differs from the negatively selecting cognate OVA specificity (SIINFEKL) by a single N to R amino acid substitution at the p4 position.

**PreTCR Binding to pMHC Ligands Is Force-Dependent.** We next ascertained whether the preTCR displays a dynamic binding response under force as seen for the mature αβTCR using BFP (18). For N15αβ, TCR–pMHC bond lifetime increases with application of force, reaches a maximum at 10 pN, and then decreases as additional force is applied (Fig. 3*D*), characteristic of catch bond formation. The N15β WT preTCR (pTα-β WT) shows a weaker catch bond at 10 pN (0.6-s peak lifetime) but nevertheless manifests peak equivalent bond lifetime to the OT1 αβTCR (Fig. 3*D*). Both $\beta M2_2$- and $\beta M2_3$-containing preTCRs form catch bonds with pMHC only below 5 pN force but slip bonds thereafter, which is characterized by increasing force linked to accelerated bond release (Fig. 3*E*). Bond lifetime modification by force is not unexpected (18, 19, 30) and is not correlated with force-free 3D (31–33) or 2D measurements (28, 34). Thus, prolonged bond lifetime for $M2_3$ under force compared with $M2_2$ is not inconsistent with the solution NMR analyses, where binding is force-free and occurs in the absence of biomembrane constraints. N30β WT, in contrast to N15β WT, shows only slip bonds effectively at and above 5 pN (Fig. 3*F*), although at all forces, the bond lifetime for CDR1 and -2 mutated N30β (M12) remains shorter than for the N30β WT. N15β $MP_3$ displays a force lifetime profile similar to that of the $M2_2$ and $M2_3$ mutants (Fig. S5*F*), suggesting that both CDR and patch regions contribute to the mechanism of the catch bond in the preTCR.

**PreTCR Ligation by pMHC Initiates Calcium Flux.** It has been previously reported that the calcium response of pre-T cells remains intact after triggering with anti-CD3 antibodies (35), a phenomenon that we recapitulated in β-transduced SCID.adh cells (Fig. S6*A*). Moreover, the presence of mutations within β does not affect the ability of the preTCR complex to signal through CD3, indicating that each construct is part of a functional cell surface receptor (35). To determine if pMHC ligand could activate $Ca^{2+}$ flux in the same cells, N15β WT preTCR-expressing SCID.adh cells were individually monitored for $Ca^{2+}$ triggering (Fig. 3 *G* and *H*) after loading into a microfluidic device (36) with VSV8/$K^b$ (Fig. 3 *G*, Upper and *H*, Upper) or BSA control protein (Fig. 3 *G*, *Lower* and *H*, *Lower*) coupled to the surfaces. N15β WT robustly drives signaling in the presence of VSV8/$K^b$, which was revealed by the comparison of $Ca^{2+}$ peak intensity measurements (Fig. 3*I*). Untransduced SCID.adh cells are not activated by either control or VSV8/$K^b$-coupled surfaces (Fig. S6 *B* and *C*). Mutagenesis of CDR2 partially abrogates $Ca^{2+}$ flux generated by interaction with VSV8/$K^b$-treated surfaces (Fig. S6 *D* and *E*).

**Thymocyte Development Is Impacted by preTCR β-Chain CDR or Patch Mutations.** To test whether Vβ CDR2 mutations impact DN thymocyte proliferation and developmental progression, progenitor stem cells were cultured on OP9-DL4 stroma after isolation from fetal livers of B6 *Rag2*$^{-/-}$ mice, progression to the DN3 stage, retroviral transduction with β, and FACS sorting as described (37). The kinetics of thymocyte expansion as well as progression from DN3 to DP were then followed (Fig. S7). With the OP9 parental cell line lacking the Notch ligand DL4, essentially no proliferation or development is observed (Fig. 4*A* and Fig. S7). However, when placed on the OP9-DL4 cultures, a 2,500-fold expansion occurs for WT N15β-transduced thymocytes but not for vector controls (Fig. 4*A* and Figs. S7 and S8), recapitulating previous findings regarding the importance of both Notch and preTCR signaling in development. The total number of cells after 10 d of culture was greater for the WT N15β or $M2_3$ β-transduced cultures compared with the mutant $M2_2$β (Fig. 4*A*). This difference is because of an apparent proliferative advantage within the DN3 stage, resulting in more cells transitioning through DN4 and CD8 immature single positive into DP (Fig. 4*B*). When comparing numbers of cells transitioned from DN3 to DN4 and beyond relative to WT, significantly fewer cells bearing the $M2_2$ mutation but similar numbers of $M2_3$ cells were found after 6–7 d in culture (Fig. 4*C*), suggesting a significant role for ligand recognition within the DN3 to DP developmental transition. Using N30β, we found deficiencies in developmental progress for mutants of CDR3 (M3) and combined mutation of CDR1 and -2 (M12) and CDR1, -2, and -3 (M123) but not individual mutagenesis of CDR1 or -2 (M1 or M2, respectively) (Fig. 4*D*). N30β also produced significantly more developed cells than N15β in this system (Fig. 4*D*). When residues within the Vβ patch region are mutated to alanine in N15β, progressively fewer cells successfully transitioned beyond DN3 as more residues within the patch were altered (Fig. 4*E*). Cell surface expression levels could not account for differences between WT and mutated β-subunits (Fig. S9 *A*–*C*). Apoptosis was prevalent in nondividing cells relative to those that were proliferating rapidly (Fig. S9*D*), but developed cellularity was not caused by any direct change in apoptotic rate between WT- and mutant-β, because Annexin levels showed no dependence on β-subunit identity (Fig. S9*E*). The OP9-DL4 stromal cell findings were validated in a separate assay using a two-color retroviral internal ribosome entry site (IRES) system, allowing control of interlobe variability within the fetal

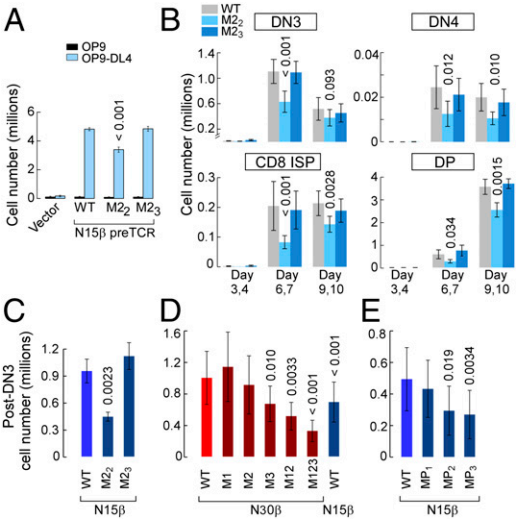


**Fig. 4.** PreTCRβ CDR or Vβ patch mutations modulate proliferation within DN3 and progression from DN3 to DP stages of β-transduced thymocytes in stromal cell systems. (*A*–*C*) Developmental effects of CDR2 mutagenesis on N15β-transduced thymocytes; 2,000 sorted DN3 B6 Rag2$^{-/-}$ thymocytes were cultured in the OP9-DL4 system for 9–10 d. Results are shown as averages ± SEMs ($n$ = 4). (*A*) Total thymocyte numbers at the end of OP9 or OP9-DL4 cultures. (*B*) Thymocyte numbers in OP9-DL4 cultures at DN3, DN4, CD8 immature single positive (ISP), and DP developmental stages at days 3 and 4, days 6 and 7, or days 9 and 10. (*C*–*E*) Number of cells developed beyond DN3 at days 6 and 7 within OP9-DL4 cultures of N15β- or N30β-transduced B6 Rag2$^{-/-}$ thymocytes. Significance of difference with leftmost β-WT is shown above each bar. (*C*) Developed cells for N15β WT vs. CDR2 mutants. (*D*) N30β WT vs. CDR mutants and N15β WT ($n$ = 7). (*E*) N15β WT vs. Vβ patch mutants ($n$ = 7).

thymic organ culture system, which recapitulates a more complete thymic inductive environment (Fig. S9*F*) (38). In this assay as well, the $M2_2$ β-chain attained lesser cellularity than WT N15β, whereas the $M2_3$ β-chain did not differ significantly from WT (Fig. S9*G*).

## Discussion

Our experiments clarify some fundamental features of early thymic development (Fig. 5). The β-chain has the interesting dual role of being a structural component of both the preTCR and the mature αβTCR. PreTCR function is critical for αβ–T-cell development but not that of the γδ–T-cell lineage (10). Clearly, β alone or within the context of the preTCR binds ligand in a specific manner as shown by several independent techniques: NMR studies (Figs. 1 and 2), 2D affinity measurement, and BFP analysis (Fig. 3 *A*–*F*). This engagement engenders $Ca^{2+}$ flux (Fig. 3 *G*–*I*), which is known to be a critical step in TCR signaling. Certainly, our results do not dispute the prevailing view that productive β-gene rearrangement and expression drive development to the DP stage (Fig. 4*A*). Because early studies showed that this DN to DP progression proceeds in the absence of an external pMHC ligand and is observed in DN thymocytes with preTCR complexes lacking pTα and -β ectodomains, preTCR-driven DP development is not absolutely dependent on pMHC interaction (39). Rather, the nature of the repertoire may be affected by preTCR–pMHC binding. We find that a given β expressing thymocyte may proliferate more readily within the DN3 stage than another closely related variant (Fig. 4), altering the numeric representation of that particular β-clonotype during subsequent TCRα rearrangement. This finding is consistent with an initial optimization of the TCRαβ repertoire by preselecting clonotypes with a predisposition for pMHC interaction. The results presented here also importantly indicate reduced peptide stringency involved in β-selection, which was pointed to by the decreased binding of VSV8/$K^b$ by both $M2_2$ and $M2_3$ mutants (Fig. 2 *E* and *F*), despite the comparable efficiency of $M2_3$ to WT N15β when assayed in thymic culture (Fig. 4 *A*–*C*).

These data underscore the broader specificities measured by BFP (Fig. 3*A*) as well as the force-driven changes modulating preTCR–pMHC bond lifetime. Thus, in addition to facilitating DP thymocyte progression through an apparently autonomous preTCR signaling mechanism (39), preTCR interaction with pMHC and/or additional ligands tunes selection of β-chains to be used by αβTCR-expressing DP thymocytes. Future research will show the relationships between autonomous preTCR signaling, Notch signaling, and preTCR–pMHC interactions in modulating early development under different piconewton force conditions that may be encountered intrathymically (Fig. 5). Perhaps the capacity of preTCR-expressing DN3 and -4 and early DP thymocytes to ligate multiple specificities increases the likelihood of developmental progression by promoting signaling that would otherwise be too infrequent if restricted to a single ligand. Of note, neither the previously reported superdomain of two antiparallel preTCRs model (13) nor the upright Vβ dimer model (14) represents the geometry of this pMHC binding competent receptor. Although the former's orientation makes the CDRs inaccessible and both models occlude the hydrophobic patch implicated in ligand binding, a monomer-competent/dimer-incompetent equilibrium cannot be excluded. Nonetheless, ligand-gated signaling is essential here for preTCR-bearing cells, because spontaneous $Ca^{2+}$ flux is not observed (Fig. 3 and Fig. S6).

Using optical tweezers and DNA tether spacer technology, which permit piconewton force application and nanometer-scale precision, Das et al. (19) determined how bioforces relate to self- vs. nonself-discrimination. Single-molecule analyses involving isolated αβ-heterodimers as well as complete TCR complexes on T lymphocytes revealed that the FG loop in the β-subunit constant domain allosterically controls both the variable domain module's catch bond lifetime and peptide discrimination through force-driven conformational transition. Of interest and in contrast to integrins, the TCR interrogates its ligand through a strong force-loaded state, with release through a weakened extended state. Given the presence of the FG loop in the preTCR, a similar mechanism is likely operative. Molecular details of the role of the Vβ hydrophobic patch in ligand binding geometry will illuminate how force transduction through the β-subunit diverges relative to the mature αβTCR (19). In the preTCR, the unpaired Vβ domain is likely to behave differently under force compared with when it is in the context of the paired TCRαβ V module.

Given that β-gene rearrangement, like that in other TCR and B-cell receptor (BCR) genes, involves a stochastic process generating myriad specificities but at the cost of engendering either no pMHC reactivity or excess unwanted autoreactivity, an early competitive first-cut (i.e., coarse) selection process to enhance the incorporation of valuable β-chains into αβTCRs makes teleological sense. This preselection process imparted by the β-chain at the DN stage may relate to the propensity of certain individual β-subunits to participate in self-pMHC interactions that may be favored, expanding those preTCR-bearing cells. The fact that N30β but not N15β is incorporated into the dominant B6 response to VSV8/$K^b$ is noteworthy (22). Whether excessively strong pMHC interactions disfavor DN development through apoptotic mechanisms is not excluded and requires additional study. Notwithstanding, our findings suggest that tuning of the αβTCR repertoire begins before the DP thymocyte stage with β-selection that is modulated by self-ligands.

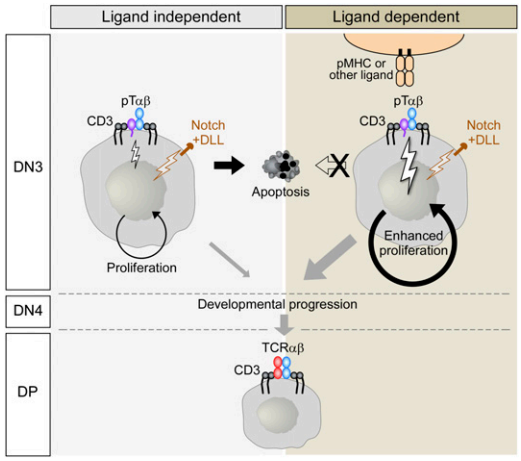


**Fig. 5.** Model for early DN thymocyte selection through ligand-independent and -dependent processes. Interactions with thymic ligands occur in a background of DL-4–dependent Notch signaling as well as constitutive preTCR signaling. Nonetheless, signaling is enhanced through preTCR–ligand interactions, leading to greater proliferation in the DN3 stage. Apoptosis occurs predominantly in nondividing thymocytes. Note that the possibility of non-MHC ligands is indicated, because this has not been excluded experimentally. For simplicity, CD3ζ has been omitted. DLL, Delta-like ligand.

## Materials and Methods

**Protein Expression and Purification.** β-Proteins were expressed in *Escherichia coli* using M9 minimal media containing $^{15}N$ $NH_4$-Cl, $^{2}H$-$^{13}C$-glucose, and 99.9% (mol/mol) $D_2O$ for backbone assignments and cross-saturation experiments or $^{15}N$ $HN_4Cl$ for HSQC titration experiments (23, 25). TCRβ (14), VSV8/$K^b$ (40), and CD3γε (41) were produced as previously described. pMHC in micropipette experiments was generated with C-terminal biotin tags and produced by the NIH Tetramer Core Facility at Emory University. Mutations generated for proteins are detailed in *SI Materials and Methods*.

**NMR.** Standard experiments were used on Bruker 900-, 800-, 750-, 600-, or 500-MHz or Agilent 600-MHz NMR machines equipped with cryogenic probes. Data were processed using NMRPipe (42), and they were analyzed and displayed using CARA (43). Molecular models were created with PyMol (44). Additional details are in *SI Materials and Methods*.

**Micropipette Adhesion Frequency Analysis.** The micropipette adhesion frequency assay was used to measure effective 2D affinity (34, 45). In brief, monomeric pMHC was coated onto RBCs using biotin–streptavidin coupling. An RBC and an SCID.adh cell were aspirated by respective micropipettes, and contact time-dependent adhesion frequencies were measured as described in *SI Materials and Methods*.

**BFP Force-Clamp Assay.** Two assays were conducted using BFP: a thermal fluctuation assay (34, 46, 47) for zero-force off-rate measurement and a force-clamp assay (18) for force-dependent bond lifetime measurement. Details of measurements and rate calculations are given in *SI Materials and Methods*.

**Microfluidics-Based Calcium Flux.** For single-cell analysis, a microfluidics-based cell trap array chip was used for calcium imaging at 37 °C as described (36), with additional details included in *SI Materials and Methods*.

**Retroviral Constructs and Transduction of Thymocytes and Fetal Liver Hematopoietic Progenitors.** Retroviral constructs coding for murine TCRβ (WT or CDR loop mutants) were inserted into the retroviral vector pLZRS-IRES-EGFP. Thymocytes originated from C57BL/6 *Rag2*$^{-/-}$ mice were transduced with N15β retroviral supernatant using Lipofectamine Reagent (Invitrogen). Additional details are given in *SI Materials and Methods*.

**OP9-DL4 Stromal Cell Culture.** OP9 and OP9-DL4 stromal cell cultures were conducted as described (48). Generally, 2,000 transduced DN3 cells (*SI Materials and Methods*) were seeded into six-well culture dishes containing stromal cells and cultured for up to 10 d.

**Flow Cytometry Analysis and FACS.** Data for fetal thymic organ culture samples, OP9 cultured samples, and SCID.adh samples were collected on a FACSAria I (BD Biosciences) and sorted or gated based on forward scatter or side scatter and appropriate fluorescent parameters as described in *SI Materials and Methods*.

Data processing and analyses for all FACS experiments used FlowJo software (TreeStar, Inc.).

**ACKNOWLEDGMENTS.** We thank Juan Carlos Zuniga-Pflücker for OP9 and OP9-DL4 cell lines; the NIH Tetramer Core Facility at Emory University for providing biotinylated peptides bound to MHC molecules monomers; Rafael A. Irizarry for statistical consultation; Bo Zhao, Jingang Gui, Baoyu Liu, and Wei Chen for assistance with preliminary experiments; and Matthew J. Lang (M.J.L.) for discussion. This work was supported by NIH Grants R01AI088023 (to H.L.), R01AI044902 (to C.Z.), P01GM04746 (to G.W.), R01AI37581 (to G.W.), R01AI19807 (to E.L.R.), and R01AI100643 (to M.J.L. and E.L.R.) and National Science Foundation Grant CBET 0954578 (to H.L.).

1. Prockop S, Petrie HT (2000) Cell migration and the anatomic control of thymocyte precursor differentiation. *Semin Immunol* 12(5):435–444.
2. Shah DK, Zúñiga-Pflücker JC (2014) An overview of the intrathymic intricacies of T cell development. *J Immunol* 192(9):4017–4023.
3. von Boehmer H (2014) The thymus in immunity and in malignancy. *Cancer Immunol Res* 2(7):592–597.
4. Mathis D, Benoist C (2009) Aire. *Annu Rev Immunol* 27:287–312.
5. Goldrath AW, Bevan MJ (1999) Selecting and maintaining a diverse T-cell repertoire. *Nature* 402(6759):255–262.
6. Shortman K, Jackson H (1974) The differentiation of T lymphocytes. I. Proliferation kinetics and interrelationships of subpopulations of mouse thymus cells. *Cell Immunol* 12(2):230–246.
7. Love PE, Bhandoola A (2011) Signal integration and crosstalk during thymocyte migration and emigration. *Nat Rev Immunol* 11(7):469–477.
8. Choi YI, et al. (2014) Dynamic control of β1 integrin adhesion by the plexinD1-sema3E axis. *Proc Natl Acad Sci USA* 111(1):379–384.
9. Halkias J, Melichar HJ, Taylor KT, Robey EA (2014) Tracking migration during human T cell development. *Cell Mol Life Sci* 71(16):3101–3117.
10. Kreslavsky T, et al. (2012) β-Selection-induced proliferation is required for αβ T cell differentiation. *Immunity* 37(5):840–853.
11. Lind EF, Prockop SE, Porritt HE, Petrie HT (2001) Mapping precursor movement through the postnatal thymus reveals specific microenvironments supporting defined stages of early lymphoid development. *J Exp Med* 194(2):127–134.
12. Yamasaki S, et al. (2006) Mechanistic basis of pre-T cell receptor-mediated autonomous signaling critical for thymocyte development. *Nat Immunol* 7(1):67–75.
13. Pang SS, et al. (2010) The structural basis for autonomous dimerization of the pre-T-cell antigen receptor. *Nature* 467(7317):844–848.
14. Zhou B, et al. (2011) A conserved hydrophobic patch on Vβ domains revealed by TCRβ chain crystal structures: Implications for pre-TCR dimerization. *Front Immunol* 2:5.
15. Desmyter A, et al. (1996) Crystal structure of a camel single-domain VH antibody fragment in complex with lysozyme. *Nat Struct Biol* 3(9):803–811.
16. Ward ES, Güssow D, Griffiths AD, Jones PT, Winter G (1989) Binding activities of a repertoire of single immunoglobulin variable domains secreted from Escherichia coli. *Nature* 341(6242):544–546.
17. Malchiodi EL, et al. (1995) Superantigen binding to a T cell receptor beta chain of known three-dimensional structure. *J Exp Med* 182(6):1833–1845.
18. Liu B, Chen W, Evavold BD, Zhu C (2014) Accumulation of dynamic catch bonds between TCR and agonist peptide-MHC triggers T cell signaling. *Cell* 157(2):357–368.
19. Das DK, et al. (2015) Force-dependent transition in the T-cell receptor β-subunit allosterically regulates peptide discrimination and pMHC bond lifetime. *Proc Natl Acad Sci USA* 112(5):1517–1522.
20. Wang J, et al. (1998) Atomic structure of an alphabeta T cell receptor (TCR) heterodimer in complex with an anti-TCR fab fragment derived from a mitogenic antibody. *EMBO J* 17(1):10–26.
21. Bentley GA, Boulot G, Karjalainen K, Mariuzza RA (1995) Crystal structure of the beta chain of a T cell antigen receptor. *Science* 267(5206):1984–1987.
22. Imarai M, Goyarts EC, van Bleek GM, Nathenson SG (1995) Diversity of T cell receptors specific for the VSV antigenic peptide (N52-59) bound by the H-2Kb class I molecule. *Cell Immunol* 160(1):33–42.
23. Marintchev A, Frueh D, Wagner G (2007) NMR methods for studying protein-protein interactions involved in translation initiation. *Methods Enzymol* 430:283–331.
24. Yin Y, Wang XX, Mariuzza RA (2012) Crystal structure of a complete ternary complex of T-cell receptor, peptide-MHC, and CD4. *Proc Natl Acad Sci USA* 109(14):5405–5410.
25. Takahashi H, Nakanishi T, Kami K, Arata Y, Shimada I (2000) A novel NMR method for determining the interfaces of large protein-protein complexes. *Nat Struct Biol* 7(3):220–223.
26. Varani L, et al. (2007) Solution mapping of T cell receptor docking footprints on peptide-MHC. *Proc Natl Acad Sci USA* 104(32):13080–13085.
27. Scott-Browne JP, White J, Kappler JW, Gapin L, Marrack P (2009) Germline-encoded amino acids in the alphabeta T-cell receptor control thymic selection. *Nature* 458(7241):1043–1046.
28. Adams JJ, et al. (2011) T cell receptor signaling is limited by docking geometry to peptide-major histocompatibility complex. *Immunity* 35(5):681–693.
29. Hogquist KA, et al. (1994) T cell receptor antagonist peptides induce positive selection. *Cell* 76(1):17–27.
30. Wang JH, Reinherz EL (2012) The structural basis of αβ T-lineage immune recognition: TCR docking topologies, mechanotransduction, and co-receptor function. *Immunol Rev* 250(1):102–119.
31. Alam SM, et al. (1996) T-cell-receptor affinity and thymocyte positive selection. *Nature* 381(6583):616–620.
32. Gascoigne NR, Zal T, Alam SM (2001) T-cell receptor binding kinetics in T-cell development and activation. *Expert Rev Mol Med* 2001:1–17.
33. Aleksic M, et al. (2010) Dependence of T cell antigen recognition on T cell receptor-peptide MHC confinement time. *Immunity* 32(2):163–174.
34. Huang J, et al. (2010) The kinetics of two-dimensional TCR and pMHC interactions determine T-cell responsiveness. *Nature* 464(7290):932–936.
35. Shinkai Y, Alt FW (1994) CD3 epsilon-mediated signals rescue the development of CD4+CD8+ thymocytes in RAG-2-/- mice in the absence of TCR beta chain expression. *Int Immunol* 6(7):995–1001.
36. Chung K, Rivet CA, Kemp ML, Lu H (2011) Imaging single-cell signaling dynamics with a deterministic high-density single-cell trap array. *Anal Chem* 83(18):7044–7052.
37. Mohtashami M, Shah DK, Kianizad K, Awong G, Zúñiga-Pflücker JC (2013) Induction of T-cell development by Delta-like 4-expressing fibroblasts. *Int Immunol* 25(10):601–611.
38. Touma M, et al. (2007) Importance of the CD3gamma ectodomain terminal beta-strand and membrane proximal stalk in thymic development and receptor assembly. *J Immunol* 178(6):3668–3679.
39. Irving BA, Alt FW, Killeen N (1998) Thymocyte development in the absence of pre-T cell receptor extracellular immunoglobulin domains. *Science* 280(5365):905–908.
40. Moody AM, Xiong Y, Chang HC, Reinherz EL (2001) The CD8alphabeta co-receptor on double-positive thymocytes binds with differing affinities to the products of distinct class I MHC loci. *Eur J Immunol* 31(9):2791–2799.
41. Sun Z-YJ, et al. (2004) Solution structure of the CD3epsilondelta ectodomain and comparison with CD3epsilongamma as a basis for modeling T cell receptor topology and signaling. *Proc Natl Acad Sci USA* 101(48):16867–16872.
42. Delaglio F, et al. (1995) NMRPipe: A multidimensional spectral processing system based on UNIX pipes. *J Biomol NMR* 6(3):277–293.
43. Keller R (2004) *Computer Aided Resonance Assignment Tutorial* (Cantina, Goldau, Switzerland).
44. Schrödinger LLC (2010) The PyMOL Molecular Graphics System (Schrödinger LLC, Cambridge, MA), Version 1.3r1.
45. Chesla SE, Selvaraj P, Zhu C (1998) Measuring two-dimensional receptor-ligand binding kinetics by micropipette. *Biophys J* 75(3):1553–1572.
46. Chen W, Zarnitsyna VI, Sarangapani KK, Huang J, Zhu C (2008) Measuring receptor-ligand binding kinetics on cell surfaces: From adhesion frequency to thermal fluctuation methods. *Cell Mol Bioeng* 1(4):276–288.
47. Chen W, Evans EA, McEver RP, Zhu C (2008) Monitoring receptor-ligand interactions between surfaces by thermal fluctuations. *Biophys J* 94(2):694–701.
48. Mohtashami M, et al. (2010) Direct comparison of Dll1- and Dll4-mediated Notch activation levels shows differential lymphomyeloid lineage commitment outcomes. *J Immunol* 185(2):867–876.
49. Angulo J, Enríquez-Navas PM, Nieto PM (2010) Ligand-receptor binding affinities from saturation transfer difference (STD) NMR spectroscopy: The binding isotherm of STD initial growth rates. *Chemistry* 16(26):7803–7812.
50. R Core Team (2014) R: A Language and Environment for Statistical Computing (R, Vienna).